79-274

Note: This is a draft of a paper being submitted for publication.
Contents of this paper should not be quoted nor referred to
without permission of the authors.   CONF-791112--54

MACROSCOPIC THEORY OF PULSED LASER ANNEALING

R. F. Wood, J. C. Wang, G. E. Giles and J. R. Kirkpatrick

MACROSCOPIC THEORY OF PULSED LASER ANNEALING

R. F. Wood and J. C. Wang
Solid State Division, Oak Ridge National Laboratory
Oak Ridge, Tennessee

G. E. Giles and J. R. Kirkpatrick
Computer Sciences Division, Oak Ridge National Laboratory
Oak Ridge, Tennessee

Radiation from high-power Q-switched lasers has been used recently in semiconductor research to anneal the lattice damage caused by ion implantation, diffuse surface-deposited dopant films, recrystallize doped amorphous films deposited on substrates, and remove precipitates present after conventional high-temperature dopant diffusion. All of these processes can be understood in terms of models based on macroscopic diffusion equations for heat and mass transport, cast in a finite-difference form to allow for the temperature- and spatial-dependence of the thermal conductivity, absorption coefficient, reflectivity, and other quantities. Results of calculations on silicon with the models show that the near-surface region of a sample can melt and stay molten for times of the order of 100 nsec during which dopant diffusion in the liquid state and nonequilibrium segregation during ultrarapid recrystallization are sufficient to explain the major features of the experimental results. In this paper, brief descriptions of the physical and mathematical models and some of the results obtained with them will be given, with particular emphasis on segregation effects.

I. INTRODUCTION

We restrict our attention here to the melting model of pulsed laser annealing because we believe the experimental evidence is overwhelmingly in favor of it. The reflectivity change exhibited by semiconductors during intense laser irradiation has been studied since about 1964. In some of the earlier papers, this reflectivity change was attributed to the high density of photogenerated carriers, i.e., to an electron-hole plasma. However, Blinov et al. (1) realized

already in 1967 that this explanation did not fit their data on the absorption of long wavelength radiation during irradiation of Si and GaAs with a high-powered Q-switched ruby laser. They concluded instead that the reflectivity change was due to the melting of a thin surface layer. A crucial question for the applicability of the melting model, at least in the form used here, concerns the lifetime of electron-hole pairs during intense laser irradiation and the transfer of energy from the electronic system to the lattice. There is a substantial body of literature on this topic and virtually all of the experimental data indicate that the electron-hole recombination time is between .01 nsec and 1 nsec. In fact, Svantesson et al. (2) found that in silicon the pulse width and shape of the recombination radiation in the region around 1.1 eV (band gap of silicon) tracked the excitation pulse ($\sim$ 30 nsec) almost identically. From the decay characteristics of the radiation, the authors concluded that the extremely fast recombination was due to Auger processes. In the earliest Soviet literature on laser annealing (3) it was recognized that melting of the near-surface region might explain the experimental results on dopant profile spreading. However, the results were not always consistent and this led some of the Soviet investigators (4) to assert that thermal models alone could not explain their results. These early experiments were done under conditions which were not ideal and the dopant profiling was done almost exclusively by anodic oxidation and stripping rather than by Rutherford backscattering and SIMS (secondary ion mass spectroscopy) techniques. Furthermore, no detailed numerical calculations of temperature profiles, motion of the liquid-solid interface, and dopant redistribution were carried out. In fact, the calculations of Wang et al. (5) to explain experimental data obtained at Oak Ridge were the first to show convincingly that the near-surface region could melt and that dopant diffusion in the molten state could explain the profile spreading which is observed. Similar calculations carried out independently by Baeri et al. (6) to explain their experimental data also appeared at approximately the same time and almost simultaneously experiments reported by Auston et al. (7) on the reflectivity change during laser annealing gave rather conclusive evidence that surface melting did occur. Since these experiments and calculations numerous other papers have appeared which support the melting model. Of course, it is possible inspite of the experimental evidence to the contrary to maintain that melting does not occur, that the reflectivity change is due solely to the very high density of laser-excited free carriers, and that some form of "radiation enhanced" diffusion is entirely responsible for the long-range diffusion of dopants. A theory

along such lines would have in the end to give almost iden-
tical results to the theory discussed here. Although it
seems unlikely to us that such a theory can be constructed,
it is certainly true that the effects of very high carrier
densities need to be considered in the development of the
melting model.

II. HEAT TRANSFER CALCULATIONS

Heat Diffusion Equations

We consider a sample irradiated with a single pulse of a
Q-switched laser. The geometry of the sample and of the
annealing configuration is such that ideally the heat conduc-
tion problem is well represented by the one-dimensional dif-
fusion equation with a heat generation function determined by
the interaction of the laser radiation and the sample. In
simplest form for a sample in which the materials parameters
are a constant, we can write the equation for the temperature
$T(x,t)$ as

$$\frac{\partial T(x,t)}{\partial t} - D_t \frac{\partial^2 T(x,t)}{\partial x^2} = P(x,t) , \qquad (1)$$

in which $P(x,t)$ is the heat generation function. D_t is the
thermal diffusion coefficient which involves the thermal con-
ductivity, the specific heat and the density of the sample
material. In laser annealing, the temperature of the sample
is raised in a few nanoseconds to the melting point and even
through the vaporization point if the laser pulse is suf-
ficiently energetic. Both the thermal conductivity K, and
the specific heat of Si are highly temperature dependent (8).
Equation 1 cannot describe such a situation and a more
complex formulation of the problem based on finite differ-
ences is required. We found that a general purpose heat con-
duction computer program, HEATING5, (9) was easily adapted to
laser annealing studies. This program solves steady-state
and transient heat conduction problems in one, two, and three
dimensions for cartesian, cylindrical, or spherical coor-
dinates. The physical problem is approximated by a lattice
of nodes, each associated with a small volume. A set of
orthogonal planes defines the nodal system. Heat may flow
between adjacent nodes along paths parallel to each coor-
dinate axis. The system of equations describing the tem-
perature distribution is derived from a heat balance
condition at each node. For example, the finite-difference,
heat-balance equation for node i lying in the bulk of the
sample is

$$C_i \frac{T_i^{n+1} - T_i^n}{\Delta t} = P_i^n + \sum_{m=1}^{6} {}_iK_m^n(T_m^n - T_i^n) \quad . \tag{2}$$

Here, T_m^n is the temperature at node m adjacent to node i at time t_n; ${}_iK_m$ is the conductance between nodes i and m; C_i is the heat capacitance of the material in the small volume around node i, and P_i^n is the heat generation rate in this volume at time τ_n. For a three-(one) dimensional problem, one C, one P, and six (two) K's may be associated with each internal node at a particular time, t_n. By choosing the increments between lattice lines and time steps small enough, the solution to the system of equations yields an accurate approximation to the appropriate differential equation. Space- and time-dependent heat generation and temperature-dependent thermal properties are relatively easy to incorporate into finite difference calculations.

HEATING5 recognizes whether or not a node is undergoing a phase change. If it is, the node's temperature is maintained at the transition temperature until the net heat flow exceeds the node's latent heat of phase change. After the phase change, the node's temperature is again determined by the conductive heat transfer equation. The ratio of the node's heat energy above that required to just reach the transition temperature to the latent heat required for the phase change is called the transition ratio. The transition ratio can be used to locate the position of the melt front which is so important for laser annealing calculations.

Heat Generation Function, Reflectivity and Absorption Coefficient

In pulsed laser annealing, the reflectivity and absorption coefficient of the material and the energy density and pulse duration time of the laser pulse largely determine the heat generation rate at each point in the sample. The function P(x,t) in Eq. 1 can be written as

$$P(x,t) = (1-R) F(x,t) , \tag{3}$$

in which R is the reflectivity and F(x,t) can be a complex function of x,t, temperature and other materials parameters and physical phenomena. The reflectivity is also a complex function of a number of parameters describing the near-

surface region of the material. In most of our calculations on Si, we have allowed R to take on two values. One value describes the reflectivity of the surface before the laser pulse impinges on the sample and the other value gives the reflectivity after the near-surface region melts.

There are many discussions in the literature of the absorption mechanisms of intense laser radiation in solids. For our purposes the paper by Grinberg et al. (10) on the absorption of laser radiation and the creation of damage by that absorption gives a good summary. Since this topic has already been discussed at length by others (see for example the paper by von Allmen in these Proceedings), we will not dwell on it here. In addition to those effects which occur even in perfect crystals, the ion-implantation process itself alters the absorption process. In undoped, single-crystal Si, the absorption coefficient k at a wavelength of $\lambda = 0.694$ μm (ruby laser) and at low light intensities is approximately 3×10^3 cm^{-1}. Under the same conditions in amorphous Si, k increases to a value of $\sim 5 \times 10^4$ cm^{-1}. In ion-implanted Si, the lattice damage created by implantation depends on the dopant, the implantation energy, and the dose. In some cases, such as 100 keV implantation of arsenic, the near-surface region is driven almost completely amorphous. We may expect that for most implantation conditions and wavelengths of laser radiation the energy will be absorbed in both the damaged and the undamaged regions of the crystal. Finally, under intense laser irradiation it may happen that carrier diffusion effects can sometimes become significant (see the paper by E. Yoffa in these Proceedings) and these can be included approximately in terms of an effective absorption coefficient.

Definition of Two Models

Two basic models have been used in most of our heat conduction calculations. In one model the absorption coefficient is assumed to have some average, constant value throughout the sample. Such a model is suggested by a) ion-implantation of light ions such as boron in silicon where the implanted region is not made completely amorphous and the nature and extent of the damage is not very well defined; b) multipulse annealing where it is known that after the first laser pulse the damage in the implanted layer may be completely removed; and c) laser-induced melting of undoped, crystalline samples. Because of the absence of a well-defined damage layer in these cases we refer to this as the crystalline or c-model. In the second model a well-defined amorphous layer is assumed to be present. This model is expected to apply to the implantation of heavy ions into

silicon in certain energy ranges and to samples on which an amorphous layer has been deposited by sputtering, e-beam deposition, etc. In this model the absorption coefficient has one value in the damaged region and some other value in the undamaged, crystalline region. We will refer to this model as the amorphous or a-model.

The latent heat of fusion is less for amorphous silicon than for single crystal silicon and presumably the melting points differ also. Reliable information about these quantities in ion-implanted materials is not available. There are some indications that the latent heat of amorphous silicon may be roughly sixty-percent of the single crystal value and this has led to speculation that this would be an important effect in laser annealing. Our models have provisions for this difference in latent heat and we will give an example of its effect below.

Some Results of Temperature Calculations

The input data for these calculations consists of the thermal conductivity K, specific heat c, density d, reflectivity R, absorption coefficient k, latent heats of fusion (crystalline L_c and amorphous L_a) and vaporization L_v, the corresponding temperatures T_c, T_a, and T_v at which the phase changes occur, the pulse shape, duration τ_ℓ, and energy density E_ℓ, and the parameters in the expressions for the radiative and convective heat transfer from the front surface. Most of these data are readily obtained from the literature and will not be discussed here.

An example of one of the most important results of the temperature calculations is given in Fig. 1. This figure is
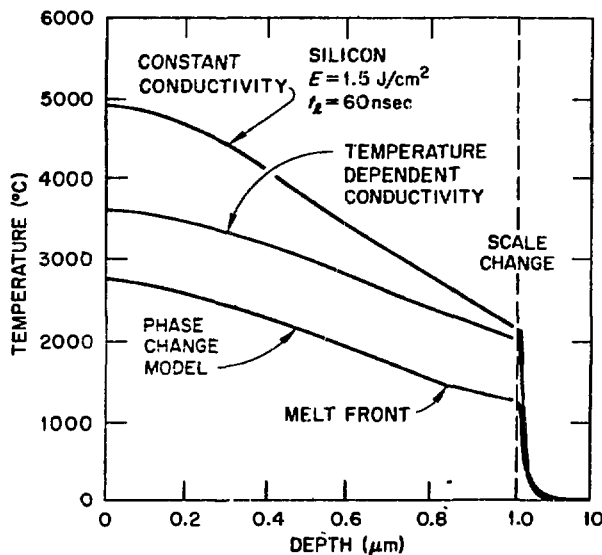

FIGURE 1.
Temperature as a function of depth for a number of approximations discussed in the text. In this figure E is the energy density and t_ℓ the duration of the incident laser pulse.

based on very early calculations which did not contain a reflectivity switch on melting; it is used here for illustrative purposes only. The top curve is a typical temperature distribution obtained from Eq. 1 when melting is not allowed and K and c are assumed to be constant with temperature. The middle curve shows the effects of including the temperature dependence of K and c. The calculations leading to the lowest curve allowed for temperature-dependent K and c and for melting. This figure shows the importance of allowing for these effects in the calculations.

From a series of calculations such as those leading to the lowest curve on Fig. 1 the melt-front position as a function of time can be obtained. Examples of such curves are shown in Fig. 2 for a 25 nsec laser pulse of various energies. Note that these calculations included a reflectivity switch from $R_s = 0.35$ (solid) to $R_m = 0.60$ (molten) on melting. The absorption coefficient is assumed to have an average value of 3×10^4 cm^{-1} throughout the material. From the curves on Fig. 2 it is found that the recrystallization velocity is of the order of 3-4 m/sec. Figures 1 and 2 provide the key to understanding the details of pulsed-laser annealing. Much of our work has been directed toward obtaining melt-front histories such as those contained in Fig. 2 for a variety of assumptions about the thermal conductivity, absorption coefficient, reflectivity, pulse duration time, etc. A more detailed account of this work will be given in a later publication (11).

In Fig. 3, we show the effects of reducing the heat of fusion in the amorphous layers, i.e., of taking $L_a < L_c$. The basic model for these calculations had $R_s = 0.35$, $R_m = 0.60$, $X_a = 0.15\mu$m (thickness of amorphous layer), $k_a = 5 \times 10^4$ cm^{-1},
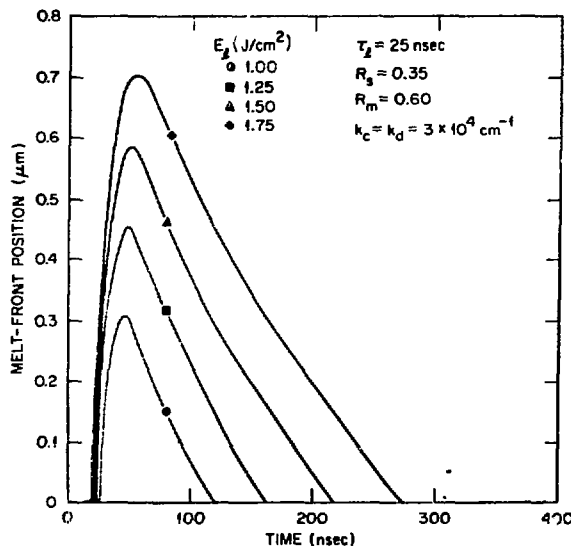

FIGURE 2
An example of the results of melt-front profile calculations.

and $k_c = 3 \times 10^3$ cm^{-1}; k_a and k_c are the absorption coefficients in the amorphous and crystalline regions respectively. Curve a gives the melt-front history for a laser pulse of $E_\ell = 1.4$ J/cm^2, $\tau_\ell = 15$ nsec, and $L_a = L_c$ and curve b is for the same conditions but with $L_a = 0.6$ L_c. Curves c and d are for the same sequence of calculations but with $E_\ell = 1.5$ J/cm^2 and $\tau_\ell = 60$ nsec. Clearly, a substantial reduction in the latent heat does not cause very large changes in the melt-front histories, as has been suggested by others. The reasons for this somewhat surprising result are quite simple and are directly related to the role played by the reflectivity switch. It should be understood that this result applies only to the conditions discussed here. The difference between L_a and L_c plays a much greater role in annealing with CW lasers where recrystallization occurs by solid-phase epitaxy.

Figure 4 is our final example of the results of heat conduction calculations; it shows the time the surface remains molten as a function of incident laser energy. The experimental data is from Auston et al. (7). The solid squares and circles give the results of calculations using sets of parameters which differ only slightly from one another. In fact, the differences are too slight to warrant discussion here. The open circles and squares are calculations more appropriate to annealing with a ruby laser ($\lambda = 0.694$ μm) and are based on an amorphous model with $X_a = 0.15$ μm and two different values of k_a. These and other calculations which we
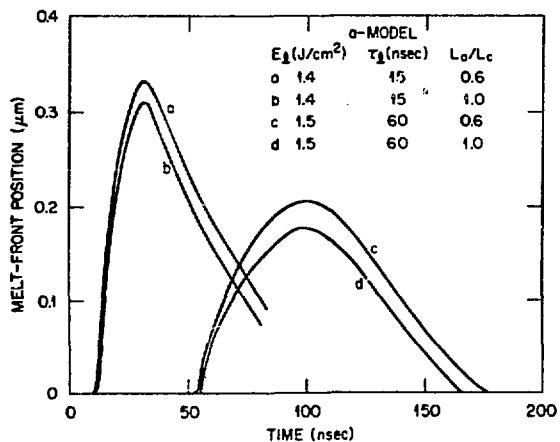

FIGURE 3. Illustrations of the effects of a latent heat reduction in the amorphous layer on melt-front profiles.
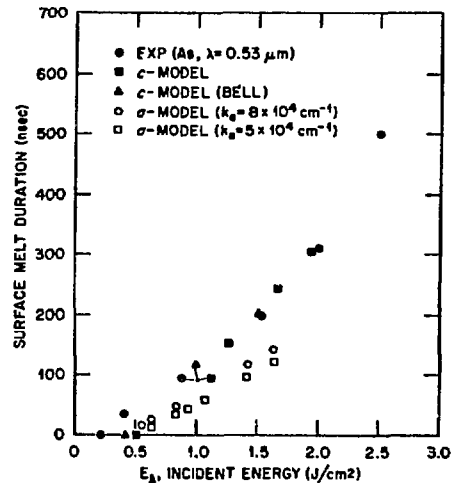
FIGURE 4. Surface melt duration as a function of incident energy for a number of different models.

have made show that the surface melt duration depends
strongly on a number of conditions under which the laser
annealing is carried out. Experimental data on the duration
of surface melting is very useful as an aid in determining
some of the parameters in a given model but such data alone
cannot uniquely determine the model to the extent that the
melt-front profile, penetration, and velocities can be pre-
dicted. The fitting of experimental dopant profiles with a
model for diffusion in the liquid state *is a great aid in the
overall development of the theory of pulsed laser annealing*
and we now consider a number of aspects of the dopant dif-
fusion problem.

III. DOPANT DIFFUSION WITHOUT SEGREGATION

As we have shown above, during pulsed laser annealing the
near-surface region of an ion-implanted sample melts. While
this region is molten, rapid diffusion of the dopant occurs
(5). In those cases where the melt front penetrates well
beyond the implanted dopant profile, rather good fits to the
experimental data can be obtained by assuming that the region
of the profile is instantaneously melted, stays molten for a
certain period of time, and then is instantaneously resoli-
dified. This "instantaneous approximation" (IA) fails when
the maximum melt-front penetration occurs within or just
beyond the implanted profile and improved approximations in
which the actual motion of the melt front is included must be
constructed. We have employed two types of approximations to
deal with this moving boundary value problem.

The first approximation is derived from the Green's func-
tion formulation of the one-dimensional, mass-diffusion
problem. In the IA, the profile after laser annealing is
given by

$$\rho(x,t) = \int_0^\infty \left[G(xt \mid x_0 t_0)\rho_i(x_0,t_0) \right]_{t_0=0} dx_0 \qquad (4)$$

in which ρ_i and ρ are the implanted and final profiles
respectively and $G(xt \mid x_0 t_0)$ is the Green's function for dif-
fusion in a semi-infinite sample. For assumed values of the
diffusion parameters, a fit of ρ to the experimental profile
determines the time during which the implanted region
remained molten. This time should be consistent with that
obtained from the calculations of temperature and melt-front
motion such as those described in the preceding section.
Obviously, when the melt-front does not penetrate beyond the

implanted profile, a single time during which the entire pro-
file is allowed to diffuse cannot be assigned in even an
approximately correct manner. A simple approximation which
gives surprisingly good results and yet remains within the
spirit of Eq. 4 is obtained from the following procedure.
From plots of the melt-front location as a function of time
such as those given in Fig. 2, the time during which any
point in the sample remains molten can be determined.
Substituting these times into a suitably modified form of
Eq. 4 and carrying out the integration over x_0 gives an
approximation to the diffused profile.

Because the approximations on which the above-described
procedure is based are difficult to justify and may not
always apply, we have used another model based on a finite-
difference formulation of the mass-diffusion equation

$$\frac{\partial \rho(x,t)}{\partial t} = \frac{\partial}{\partial x} \left[D \frac{\partial \rho(x,t)}{\partial x} \right] , \tag{5}$$

with appropriate boundary conditions. The diffusivity D can
be a function of x and t and this flexibility is used to
change from values characteristic of the liquid (D_ℓ) to those
characteristic of the solid (D_s) at the moving liquid-solid
interface. The sample is imagined to be oriented perpen-
dicular to the x axis with its front face at x=0 and its
thickness divided into cells with Δx of the order of 100 Å
or smaller. As the melt front penetrates the sample and
moves through a cell, the value of D in the cell changes from
D_s to D_ℓ. The material in all cells to the left of the melt
front is molten and diffusion occurs very rapidly within it.
When the melt front reaches its maximum penetration and
begins to recede back to the surface, solidification occurs
and the value of D in each cell is changed accordingly. The
interface segregation coefficient k_i determines the fraction
of the dopant which is incorporated into the solid. The
dopant rejected into the liquid at the interface combines
with the implanted dopant in the molten zone to give $\rho(x,t)$
of Eq. 5. The numerical methods used in the dopant diffusion
problem are similar to though not as complex as those used in
HEATING5. Brief discussions of the details of dopant dif-
fusion calculations can be found in several other papers in
these Proceedings and we will not pursue this topic further
here.

Figure 5 shows the results of dopant profile calculations
on As-implanted Si using the approximate Green's function
method described above. The experimental profiles were
measured by ion backscattering and with the possible excep-
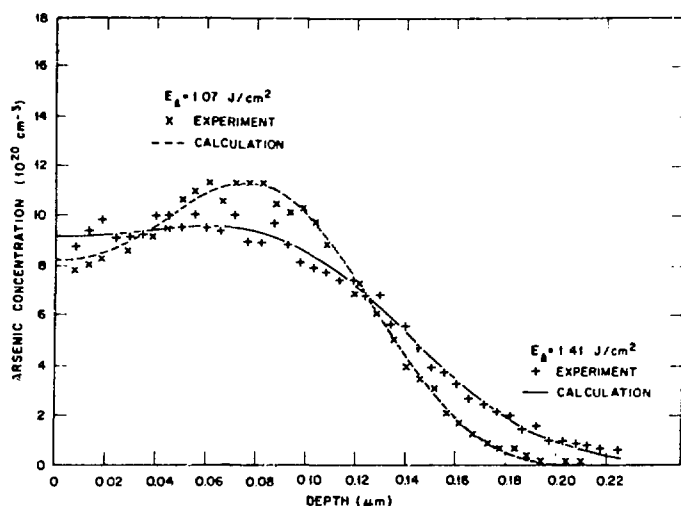tions of a very few points, the calculated curves fall within

FIGURE 5
Experimental and
calculated dopant
profiles in As-
implanted, laser-
annealed silicon.

the estimated error limits of the experiments. Dopant pro-
files obtained when As-doped amorphous layers of Si are
deposited on Si substrates and then recrystallized by laser-
induced melting are shown in Fig. 6. The experimental pro-
files in this case were determined by anodic oxidation and
stripping. The starting profiles cannot be measured by this
technique because most of the As is not electrically active
when the deposited layer is still amorphous. However, the
deposition is such that the As concentration in the deposited
layer should be nearly uniform. The uniform concentrations
required to give the calculated profiles are shown by the
dashed lines in the figure. The value of D_ℓ for As in Si was
taken from Kodera (12).

The dopant profiles in Figs. 5 and 6 were calculated with
$k_i = 1$ whereas the compilation of Trumbore (13) gives a value
of 0.3 for the equilibrium interface segregation coefficient
of As in Si. We now turn to a consideration of this discre-
pancy.

IV. NONEQUILIBRIUM SEGREGATION

In one of the earliest papers on laser annealing of ion-
implanted Si, Khaibullin et al. (3) reported that the con-
centration of dopants after annealing could exceed conven-
tional solubility limits. They recognized that this
indicated that nonequilibrium thermodynamic processes occur
during laser annealing. As we have seen in Section II, cal-
culations have shown that the near-surface regions of the
samples melt and recrystallize in times of the order of 100
nsec and that the velocity v of the liquid-solid interface
during recrystallization is of the order of 4 m/sec.
Nonequilibrium segregation effects during rapid recrystalli-
zation have been discussed in the literature on crystal
growth (14) but, until the discovery of the laser-annealing

phenomenon, the melt-front velocities attainable under well-controlled experimental conditions were too small to test various proposed models, most of which can now be shown to be inadequate or incomplete. In this Section, a simple phenomenological model which does account for the observed segregation effects is presented (15).

The interface segregation coefficient k_i for the dopant is defined as the fraction of the dopant present in the liquid at the interface that is incorporated into the solid. If equilibrium values k_i^0 were followed in the laser annealing process, then large concentration spikes at the surface would be observed for most dopants implanted in Si. Such surface spikes have not been observed for B, As and P (16,17) and satisfactory fits to the profiles can only be obtained with values of k_i nearly equal to unity (see for example Figs. 5 and 6). The fact that equilibrium solubility limits can be exceeded in systems such as these, which have retrograde solubility, can be taken as further evidence for nonequilibrium growth processes (3,14,18,19).

Recently White et al. (19) used RBS to measure the profiles of Ga, In and Bi in ion-implanted, laser-annealed Si. The results, together with earlier data on Sb and As were analyzed using a model of dopant diffusion which included segregation effects and utilized melt-front information from
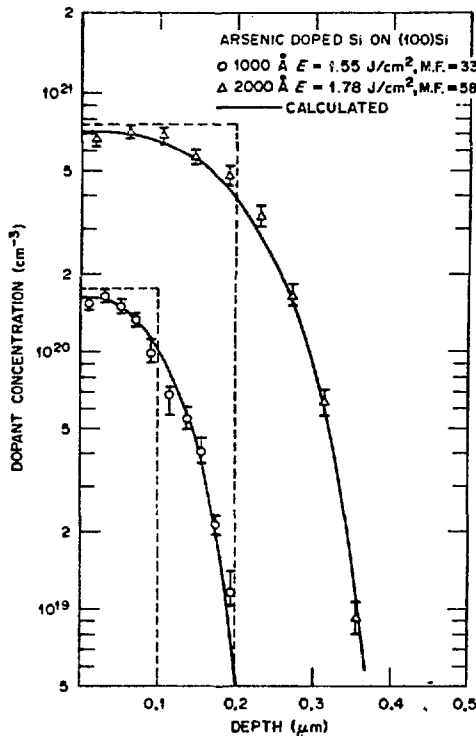

FIGURE 6. Experimental and calculated dopant profiles after laser-induced recrystallization of 1000 Å and 2000 Å layers of As-doped amorphous Si deposited on Si. In this figure E gives the incident laser energy density and M.F. the calculated maximum melt-front penetration.

calculations such as those in Section II; from fits of the measured profiles, values of k_i were extracted. The results of White et al. and of refs. 5, 16, and 17 provide data on the segregation behavior of B, P, As, Sb, Ga, In and Bi in Si during laser annealing. Values of k_i^0 and k_i are shown in Table I. The most striking feature of these data is the very large differences between k_i^0 and k_i when k_i^0 is small.

The model to be described now is based on the assumption that for $v \gg 0$ new layers of atoms may be added to the solid so quickly that dopant atoms in the interface region have a reduced probability of escape from the solid being formed. Conceptually the model is related to what Baker and Cahn (14) have referred to as "solute trapping".

The rate equations for the incorporation of host h and dopant d atoms into the solid are (20)

$$R_j^S = K_j^f C_j^L - K_j^r C_j^S \qquad , \quad j = h,d \quad , \tag{6}$$

where C_j^L and C_j^S are the concentrations of j-type atoms in the liquid and solid, and K_j^f and K_j^r are the forward (liquid $\rightarrow$ solid) and reverse rate constants in m/sec. Since the crystal grows at a rate equal to the melt front velocity, addition of the individual rate equations gives

$$v = R_h^S + R_d^S = K_h^f C_h^L + K_d^f C_d^L - (K_h^r C_h^S + K_d^r C_d^S) \tag{7}$$

with

$$C_h^S + C_d^S = C_h^L + C_d^L = 1 \quad . \tag{8}$$

It will be assumed that $K_h^f = K_d^f = K_h^{fo} = K_d^{fo}$, where K_j^{fo} is the forward rate constant under equilibrium growth conditions ($v \approx 0$); this is not a crucial assumption but it simplifies the analysis. With this assumption, Eq. (6) for $R_d^S = vC_d^S$ and

Table I. Results of calculation of k_i and comparison to experiment. In the fourth column, con.=1.75 m/sec.

Dopant	k_i^o	k_i (exp)	k_i v_o=con.	k_i v_o=D_ℓ/x_o	ΔU_d^{ra} eV	c_d^S/c_d^{So}
B	0.8	1.00	0.98	0.99	-0.032	---
P	0.35	1.00	0.90	0.95	-0.152	1.5
As	0.3	1.00	0.88	0.97	-0.175	1.4
Sb	0.023	0.7	0.68	0.88	-0.547	26
Ga	0.008	0.2	0.61	0.31	-0.700	14
In	0.0004	0.15	0:45	0.15	-1.134	400
Bi	0.0007	0.4	0:48	0.39	-1.053	1000
Al	0.0020	-	0.53	0.52	-0.901	55

Eq. (7) yield

$$K_d^{fo}C_d^S - (K_h^r - K_d^r)C_d^S(1-C_d^S) = K_d^{fo}C_d^L \quad . \tag{9}$$

Under most conditions of laser annealing C_d^S is not more than a few percent and therefore to the accuracy needed here $(1-C_d^S) \approx 1$. The interface segregation coefficient for the dopant, $k_i = C_d^S/C_d^L$, can then be expressed as

$$k_i = K_d^{fo}/(K_d^{fo} - K_h^r + K_d^r) \quad . \tag{10}$$

We assume that the rate constant K_d^r is of the usual form

$$K_d^r = A_d^r \exp(-U_d^r/RT) \quad , \tag{11}$$

in which U_d^r is the barrier height for escape of dopant atoms from the solid at the interface; similar forms are assumed for K_h^{fo} and K_h^r. Furthermore, U_d^r is assumed to be velocity dependent and written as

$$U_d^r(v) = U_d^{ro} + \Delta U_d^r(v) \quad , \tag{12}$$

where U_d^{ro} is the equilibrium value. Now ΔU_d^r may be a complicated function of v, but it must approach zero as $v \to 0$ and a constant value as v becomes large. The simple form

$$\Delta U_d^r(v) = \Delta U_d^{ra}(1 - \exp(-v/v_0)) \tag{13}$$

satisfies these conditions; ΔU_d^{ra} is the asymptotic value of ΔU_d^r as v becomes very large and v_0 is a parameter discussed below.

$$K_d^r = F \, K_d^{ro}\exp(-\Delta U_d^r(v)/RT) \tag{14}$$

with $F \equiv A_d^r/A_d^{ro}$.

Since both C_d^L and C_d^S are small, $C_h^L \approx C_h^S$, and from Eq. (6) $v \approx K_h^{fo} - K_h^r$ because of the simplifying assumption that $K_h^f = K_h^{fo}$. Rate constants have been estimated to be of the order of 100 m/sec (21). Assuming this value to be approximately valid for Si, K_h^r must be 96 m/sec to obtain $v = 4$ m/sec. The maximum value k_i can have for the systems of interest here is 1 and, with the previous assumptions that $K_d^{fo} = K_h^f$, this occurs when $K_d^r = K_h^r$. Hence, in Eq. (10) the term $K_d^{fo} - K_h^r$ compared to K_d^r can be neglected. With the definition $k_i^0 \equiv (C_d^S/C_d^L)_{v=0} = K_d^{fo}/K_d^{ro}$, Eq. (10) becomes

$$k_i = (k_i^0/F)\exp(\Delta U_d^r(v)/RT) \quad . \tag{15}$$

From the requirements that $k_i \to k_i^0$ as $v \to 0$ and $k_i \to 1$ as v becomes large, it is found that $F = 1$,

$$\Delta U_d^{ra} = - RT \ln k_i^0 , \tag{16}$$

and hence

$$k_i = k_i^0 \exp((- RT \ln k_i^0)(1-\exp(-v/v_0))/RT) \quad . \tag{17}$$

Column 4 of Table I shows the results when a single value of v_0 is used in Eq. (7). Clearly, the model can account for the extraordinarily large differences observed between k_i^0 and k_i. There is no reason v_0 should be the same for all dopants and experimentation suggested that the diffusion coefficient in the liquid D_ℓ, was a relevant parameter. Putting $v_0 = D_\ell/x_0$ and $x_0 = 225$ Å gave the results in column 5. Values of D_ℓ were taken from Kodera (12) and varied within his stated error ranges to give the fits to k_i (exp) in Table I. Only for Sb and Ga are there appreciable differences between the experimental and calculated values. Approximately 10% and 40% respectively of these dopants were lost during annealing and this made a unique fit to the experimental profiles difficult. Thus, the overall fit is remarkably good. With Eq. (17), k_i was calculated as a function of v and the results are given in Fig. 7.
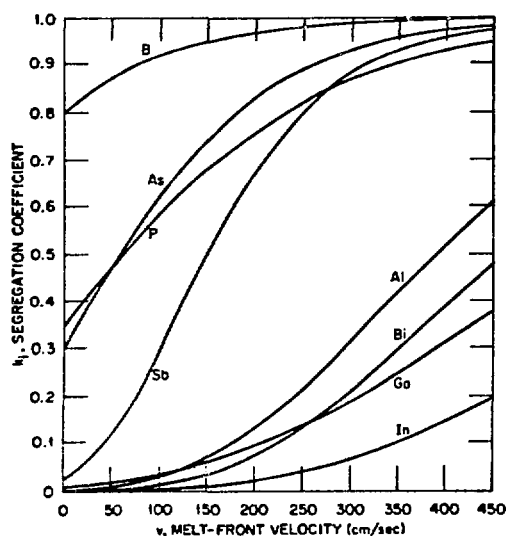

FIGURE 7. Dependence of k_i on melt-front velocity.

The equation

$$v = K_h^f \, (\Delta H_h / RT_M^2) \, \Delta T \quad , \quad \Delta T \equiv (T_m - T) \tag{18}$$

can be derived (see e.g. Thurmond, ref. 20) from Eq. 6. ΔH_h and T_M are the heat of fusion and the melting temperature respectively of the host. ΔT, the temperature drop across the interface which drives the melt front can not be discontinuous and must have a distance Δx associated with it. From the calculations of heat transport such as those in Section II that determined v, $(\partial T/\partial x)$ at the melt front can also be determined and for the conditions of the present experiments, it is $\approx 10^7$ °K/cm. Using $v = 4$ m/sec, $K_h \approx 100$ m/sec, $\Delta H_h = 12$ kcal/mole and $T_M = 1683$°K, it is found that $\Delta T \approx 20$°K and $\Delta x = 200$ Å. This calculation suggests an obvious interpretation of x_0 in $v_0 = D_\ell/x_0$, i.e., it can be equated with Δx and referred to as the width of the interface region. In the interface region, dopant diffusion is characterized by a diffusion coefficient D_i which is of the order of D_ℓ. The undercooling or supercooling given by ΔT does not depend on the dopant concentration; it is a property of pure Si. In addition, at high doping concentrations in the interface region, constitutional supercooling can be expected and may lead to the formation of cellular structures which have been observed in some cases during laser annealing.

Column 6 in Table I gives values of ΔU_d^{ra}. When these "trapping energies" are compared to the activation energy E_a for diffusion in the solid (22) it is found that ΔU_d^{ra} is a rather small fraction of E_a for the dopants listed in Table I. Thus, it is suggested that the bonding between the dopant and host atoms is easily great enough to account for the trapping. The situation is quite different for dopants such as Cu and Fe. Values of k_i^0 (ref. 13) are 4×10^{-4} and 8×10^6 respectively and the corresponding values of E_a are ~ 1 eV and 0.87 eV whereas, from Eq. (16), ΔU_d^{ra} for Cu is -1.13 eV and for Fe it is -1.70 eV. The bonding properties of Fe and Cu in Si are not sufficient to provide the necessary trapping energy.

From the relationship $C_d^L = 1 - C_h^L$ and the expression for C_h^L in an ideal dilute solution (e.g., Thurmond p. 149, ref. 20), the equation

$$C_d^S = k_i \, (1 - \exp(-\Delta H_h \Delta T / RT_M^2)) \tag{19}$$

can be obtained. With the values of k_i in column 5 of Table I and $\Delta T = 20$°K, C_d^S was calculated. The ratio of C_d^S to the maximum equilibrium solubility C_d^{So} extracted from ref. 13

are given in the last column. These ratios are in quite
satisfactory agreement with the experimental values given in
ref. 19 and in the paper by C. W. White, S. R. Wilson, and
B. R. Appleton in these Proceedings.

ACKNOWLEDGMENTS

REFERENCES

1. L. M. Blinov, V. S. Vavilov, and G. N. Galkin, Sov.
Phys. Semiconductors 1, 1124 (1967).
2. K. G. Svantesson, N. G. Nilsson, and L. Huldt, Sol.
State Comm. 9, 213 (1971).
3. I. B. Khaibullin, E. I. Shtyrkov, M. M. Zaripov, M. F.
Galyautdinov, and G. G. Zakirov, Sov. Phys. Semicond.
11, 190 (1977).
4. I. B. Khaibullin, E. I. Shtyrkov, M. M. Zaripov, R. M.
Bayazitov, and M. F. Galjautdinov, Radiat. Eff. 36, 225
(1978).
5. J. C. Wang, R. F. Wood, and P. P. Pronko, Appl. Phys.
Lett. 33, 455 (1978).
6. P. Baeri, S. U. Campisano, G. Foti, and E. Rimini, Appl.
Phys. Lett. 33, 137 (1978).
7. D. H. Auston, C. M. Surko, T.N.C. Venkatesan, R. E.
Slusher, and J. A. Golovchenko, Appl. Phys. Lett. 33,
437 (1978).
8. H. R. Shanks, P. D. Maycock, P. H. Sidles, and G. C.
Danielson, Phys. Rev. 130, 1743 (1963).
9. The HEATING5 program has been developed over ʔ period of
years at the Oak Ridge National Laboratory. It is pro-
bably quite similar to large heat conduction programs
developed at a number of other laboratories.
10. A. A. Grinberg, R. F. Mekhtiev, S. M. Ryvkin, V. M.
Salmanov, and I. D. Yaroshetskii, Sov. Phys.-Solid State
9, 1085 (1967).
11. R. F. Wood and G. E. Giles (to be submitted to Phys. Rev.).
12. H. Kodera, J. Appl. Phys. (Japan) 2, 212 (1963).
13. F. A. Trumbore, Bell System Tech. J. 39, 205 (1960).
14. J. C. Baker and J. W. Cahn, Acta Met. 17, 575 (1969).
15. This section is taken in large part from a paper
recently submitted for publication by one of us (RFW).

16. C. W. White, J. Narayan, and R. T. Young, Science 204, 461 (1979).
17. R. T. Young, J. Narayan, and R. F. Wood, Appl. Phys. Lett. 35, 447 (1979).
18. K. A. Jackson and H. J. Leamy, Laser-Solid Interactions and Laser Processing, ed. by H. J. Leamy and J. M. Poate (American Institute of Physics, New York, 1979), p. 102.
19. C. W. White, S. R. Wilson, and B. R. Appleton, J. Appl. Phys. (to be published).
20. See for example, K. A. Jackson, Can. J. Phys. 36, 683 (1958), and C. D. Thurmond in Semiconductors, ed. by N. B. Hannay (Reinhold, 1959), p. 145.
21. B. Chalmers, Trans. AIME 200, 519 (1954).
22. B. L. Sharma, Diffusion in Semiconductors, (Trans. Tech. Publications, Clausthal-Zellerfeld, Germany, 1970).